Hindawi
Advances in High Energy Physics
Volume 2020, Article ID 2453476, 8 pages
https://doi.org/10.1155/2020/2453476

Research Article

Deconfinement and Freezeout Boundaries in Equilibrium Thermal Models

Abdel Nasser Tawfik,[1,2] **Muhammad Maher**,[3] **A. H. El-Kateb**,[3] **and Sara Abdelaziz**[3]

[1]*Nile University, Egyptian Center for Theoretical Physics (ECTP), Juhayna Square of 26th-July-Corridor, 12588 Giza, Egypt*
[2]*Goethe University, Institute for Theoretical Physics (ITP), Max-von-Laue-Str. 1, D-60438 Frankfurt am Main, Germany*
[3]*Faculty of Science, Physics Department, Helwan University, 11795 Ain Helwan, Egypt*

Correspondence should be addressed to Abdel Nasser Tawfik; atawfik@nu.edu.eg

Received 9 October 2019; Accepted 28 January 2020; Published 24 February 2020

Guest Editor: Jajati K. Nayak

In different approaches, the temperature-baryon density plane of QCD matter is studied for deconfinement and chemical freezeout boundaries. Results from various heavy-ion experiments are compared with the recent lattice simulations, the effective QCD-like Polyakov linear-sigma model, and the equilibrium thermal models. Along the entire freezeout boundary, there is an excellent agreement between the thermal model calculations and the experiments. Also, the thermal model calculations agree well with the estimations deduced from the Polyakov linear-sigma model (PLSM). At low baryonic density or high energies, both deconfinement and chemical freezeout boundaries are likely coincident, and therefore, the agreement with the lattice simulations becomes excellent as well, while at large baryonic density, the two boundaries become distinguishable forming a phase where hadrons and quark-gluon plasma likely coexist.

1. Introduction

Strongly interacting matter under extreme conditions is characterized by different phases and different types of phase transitions [1]. The hadronic phase, where stable baryons build up a great part of the Universe and the entire everyday life, is a well known phase. At high temperatures and/or densities, other phases appear. For instance, at temperatures of a few MeV, chiral symmetry restoration and deconfinement transition take place, where quarks and gluons are conjectured to move almost freely within a colored phase known as the quark-gluon plasma (QGP) [2]. At low temperatures but large densities, hadronic (baryonic) matter forming compact interstellar objects such as neutron stars is indubitably observed in a conventional way, and very recently, gravitational waves from neutron star mergers have been detected, as well [3]. At higher densities, extreme interstellar objects such as quark stars are also speculated [4]. In lattice quantum chromodynamics (QCD), different orders of chiral and deconfinement transitions have be characterized, especially at low baryon densities.

The program of heavy-ion collision experiments dates back to early 1980s. Past (AGS, SIS, and SPS), current (RHIC and LHC), and future facilities (FAIR and NICA) help in answering essential questions about the thermodynamics of the strongly interacting matter and in mapping out the temperature-baryon density plane [2]. The unambiguous evidence on the formation of QGP is an example of a great empirical achievement [5, 6]. The colliding nuclei are conjectured to form a fireball that cools down by rapid expansion and finally hadronizes into individual uncorrelated hadrons. The present script focuses on the temperature-baryon density plane, concretely near the hadron-QGP boundaries, in the framework of the equilibrium thermal model [7]. To this end, we put forward a basic assumption that both directions, the hadron-QGP and QGP-hadron phases are quantum-mechanically allowed [8]. In other words, the picture drawn so far seems in fundamental conflict with the time arrow. The concept of an arrow of time prevents the reverse direction, especially if the change in the degrees of freedom or entropies aren't following the causality principle, the second law of thermodynamics. The statistical thermal approaches

work well near both deconfinement and chemical freezeout boundaries [2, 9]. This could be understood in the light of the thermal nature of an arbitrary small part of the highly entangled fireball states. Following the Eigenstate Thermalization Hypothesis [8, 10], the corresponding probability distribution of the projection of these states remains thermal. We follow the line that the thermal models reproduce well the particle yields and the thermodynamic properties of the hadronic matter including the chiral and freezeout temperatures. We compare our calculations with reliable lattice QCD simulations, an effective QCD-like approach, and available experimental results.

The present script is organized as follows. In Section 2, approaches for deconfinement and freezeout boundaries in equilibrium thermal models are introduced. The results are discussed in Section 3. Section 4 is devoted to the conclusions and outlook.

2. Equilibrium Thermal Models

It was conjectured that the formation of the hadron resonances follows the bootstrap picture, i.e., the hadron resonances or the fireballs are composed of further resonances or fireballs, which in turn are consistent of lighter resonances or smaller fireballs, and so on [11, 12]. The thermodynamic quantities of such a system can be deduced from the partition function $Z(T, \mu, V)$ of an ideal gas. In a grand canonical ensemble, this reads [2, 13–17]

$$Z(T, V, \mu) = \mathrm{Tr}\left[\exp\left(\frac{\mu N - H}{T}\right)\right], \tag{1}$$

where H is the Hamiltonian combining all relevant degrees of freedom and N is the number of constituents of the statistical ensemble. Equation (1) can be expressed as a sum over all hadron resonances taken from a recent particle data group (PDG) [18] with masses up to 2.5 GeV [19]:

$$\begin{aligned}\ln Z(T, V, \mu) &= \sum_i \ln Z_i(T, V, \mu) \\ &= V\frac{g_i}{2\pi^2}\int_0^\infty \pm p^2 dp \ln\left[1 \pm \lambda_i \exp\left(\frac{-\varepsilon_i(p)}{T}\right)\right],\end{aligned} \tag{2}$$

where the pressure reads $T\partial \ln Z(T, V, \mu)/\partial V$ and $\pm$ stands for fermions and bosons, respectively. $\varepsilon_i = (p^2 + m_i^2)^{1/2}$ is the dispersion relation and λ_i is the fugacity factor of ith particle [2].

$$\lambda_i(T, \mu) = \exp\left(\frac{B_i\mu_\mathrm{b} + S_i\mu_\mathrm{S} + Q_i\mu_\mathrm{Q}}{T}\right), \tag{3}$$

where $B_i(\mu_\mathrm{b})$, $S_i(\mu_\mathrm{S})$, and $Q_i(\mu_\mathrm{Q})$ are baryon strangeness, and electric charge quantum numbers (their corresponding chemical potentials) of the ith hadron, respectively. From a phenomenological point of view, the baryon chemical potential μ_b can be related to the nucleon-nucleon center-of-mass energy $\sqrt{s_\mathrm{NN}}$ [20]:

$$\mu_\mathrm{b} = \frac{a}{1 + b\sqrt{s_\mathrm{NN}}}, \tag{4}$$

where $a = 1.245 \pm 0.049$ GeV and $b = 0.244 \pm 0.028$ GeV^{-1}. The number and energy density, respectively, can be derived as

$$\begin{aligned} n_i(T, \mu) &= \sum_i \frac{\partial \ln Z_i(T, V, \mu)}{\partial \mu_i} \\ &= \sum_i \frac{g_i}{2\pi^2}\int_0^\infty p^2 dp \frac{1}{\exp\left[(\mu_i - \varepsilon_i(p))/T\right] \pm 1}, \\ \rho_i(T, \mu) &= \sum_i \frac{\partial \ln Z_i(T, V, \mu)}{\partial (1/T)} \\ &= \sum_i \frac{g_i}{2\pi^2}\int_0^\infty p^2 dp \frac{-\varepsilon_i(p) \pm \mu_i}{\exp\left[(\mu_i - \varepsilon_i(p))/T\right] \pm 1}. \end{aligned} \tag{5}$$

Likewise, the entropy and other thermodynamic quantities can be derived straightforwardly.

Both temperature T and the chemical potential $\mu = B_i\mu_\mathrm{b} + S_i\mu_\mathrm{S} + \cdots$ are related to each other and to $\sqrt{s_\mathrm{NN}}$ [2]. As an overall thermal equilibrium is assumed, μ_S is taken as a dependent variable to be estimated due to the strangeness conservation, i.e., at given T and μ_b, the value assigned to μ_S is the one assuring $\langle n_\mathrm{S}\rangle - \langle n_{\bar{\mathrm{S}}}\rangle = 0$. Only then is μ_S combined with T and μ_b in determining the thermodynamic quantities, such as the particle number, energy, and entropy. The chemical potentials related to other quantum charges, such as the electric charge and the third-component isospin, can also be determined as functions of T, μ_b, and μ_S, and each of them must fulfill the corresponding laws of conversation.

This research intends to distinguish between deconfinement and freezeout boundaries in equilibrium thermal models. The latter is characterized by T_χ and μ_b, which are conditioned to one of the universal freezeout conditions [21], such as constant entropy density normalized to T_χ^3 [22, 23], constant higher-order moments of the particle multiplicity [24, 25], constant trace anomaly [26], or an analogy of the Hawking-Unruh radiation [27]. The experimental estimation for T_χ and μ_b, as shown in Figure 1, proceeds through statistical fits for various particle ratios calculated in statistical thermal models. The former, the deconfinement transition, is conditioned to line-of-constant-physics, such as constant energy density, ρ [28]. The inclusion of the strange quarks seems to affect the critical temperatures, as these come up with extra hadron resonances and their thermodynamic contributions, where the mass of strange quarks is of the order of the critical temperature.

3. Results

Figure 1 depicts the freezeout and deconfinement parameters T_χ and μ_b as determined from the measurements gained

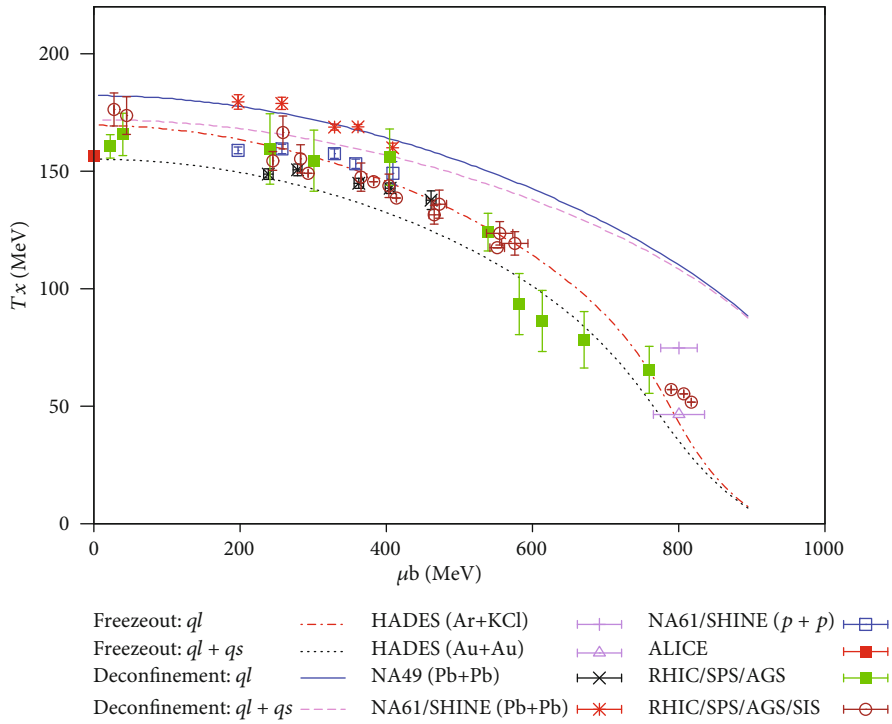

FIGURE 1: The freezeout and deconfinement parameters T_χ and μ_b as deduced from different experimental results (symbols with error bars) are depicted and confronted with the thermal model calculations for the chemical freezeout (dot-dashed and dashed curves) and deconfinement parameters (solid and long-dashed curves) with and without strange quarks.

from the following different experiments (symbols with error bars): HADES (Ar+KCal) [29], NA61/SHINE (Au+Au, $p + p$) [30–36], NA49/SHINE (Pb+Pb) [37–39], and ALICE [40–47]. In addition, analyses at RHIC/SPS/AGS [31] and RHIC/SPS/AGS/SIS energies [48–54] are combined with each other and compared with the thermal model calculations. The latter take into account both freezeout (dot-dashed and dashed curves) and deconfinement boundaries (solid and long-dashed curves) with and without strange quarks.

With the experimental results, we mean the parameters obtained when measured particle yields and/or ratios are fitted to calculations based on statistical thermal models, in which the parameters T_χ and μ_b are taken as independent variables, where the Baryon-chemical potential μ_b, for instance, can directly be fixed at a given center-of-mass energy $\sqrt{s_{NN}}$ (equation (4)). For the freezeout parameters T_χ, μ_b, μ_S, etc., the thermodynamic quantities fulfill one of the freezeout conditions reviewed in Refs. [16, 21], such as constant entropy density normalized to temperature cubed. Conditions for deconfinement phase transitions have been discussed in Refs. [16, 28], including line-of-constant-physics, such as constant energy density with varying μ_b, μ_S, and $\sqrt{s_{NN}}$. Details of the various approaches (curves) become in order now. With freezeout q_l and freezeout $q_l + q_s$, we mean QCD phase boundaries as determined under freezeout conditions, where the HRG model is configured to have only hadrons whose constituents are light quarks (q_l) and to have only hadrons with light and strange quarks ($q_l + q_s$). Under these conditions, it is likely to characterize the chemical freezeout $T - \mu_b$ plane. Furthermore, with deconfined q_l and deconfined $q_l + q_s$, we mean the line-of-constant-physics, which is defined by constant energy density, for instance. Such a line is mapped out in the HRG model in which only hadrons with light quarks (q_l) and only hadrons with light and strange quarks ($q_l + q_s$) are included.

It is obvious that both sets of freezeout parameters seem identical, for instance, at low μ_b or high $\sqrt{s_{NN}}$, where the slight difference could be tolerated. At large μ_b or low $\sqrt{s_{NN}}$, the difference between the temperatures of freezeout and deconfinement becomes larger. Such a difference would be understood based on the assumption that the chemical freezeout takes place very late after the phase of hadronization. The latter is QCD confinement transition. Its order as simulated in recent lattice QCD is a likely crossover, i.e., there is a wide range of temperatures within which QGP hadronizes or hadrons go through QGP. The time span becomes longer with the increase in μ_b or the decrease in $\sqrt{s_{NN}}$. The conjecture of the existence of a mixed phase is probably another possibility. In this phase, both types of degrees of freedom, hadrons and QGP, live together until the system goes through deconfinement to colored QGP or finally entirely freezes out to uncorrelated colorless hadrons.

The coexistence of different QCD phases was discussed in the literature, for instance in Refs. [55, 56]. The mixed QCD phases can be formed in macroscopic, mesoscopic, and microscopic mixtures. As shown in Figure 1, these mixed phases start being produced at $\sqrt{s_{NN}}$ ranging between ~5 and ~12 GeV, i.e., from $\mu_b \simeq 320$ to $\simeq 560$ MeV.

For the freezeout parameters, it is apparent that the agreement between the thermal model calculations and the

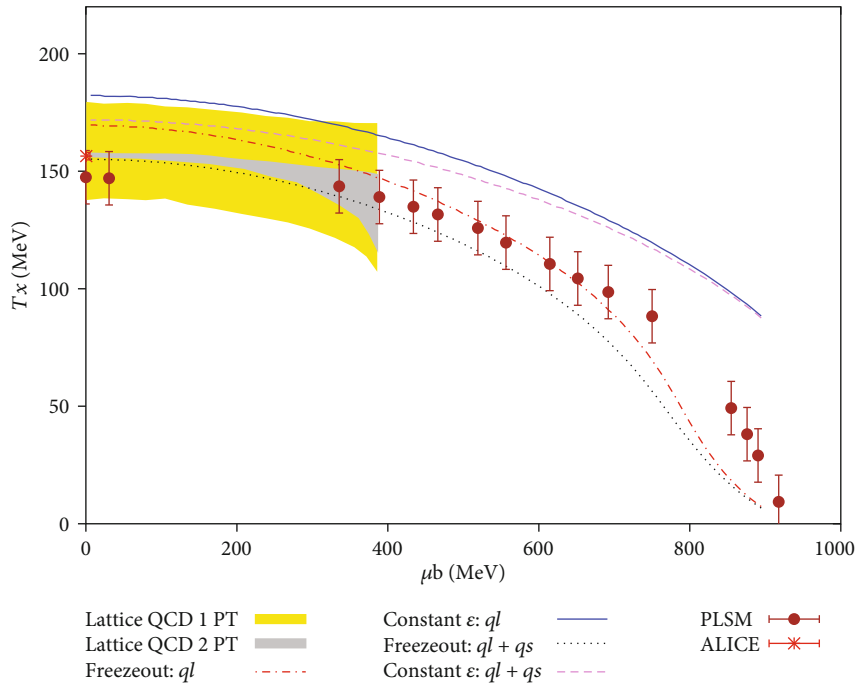

Figure 2: The same as in Figure 1, but here there is a comparison between lattice QCD simulations [61, 62] and the Polyakov linear-sigma model [63, 65–70] with the thermal model.

experimental results is very convincing. This covers the entire μ_b range and can—among other evidence—be interpreted based on the fact that the freezeout stage is the latest along the temporal evolution of the high-energy collision, where the number of produced particles is entirely fixed. The time elapsed from the stage of the chemical freezeout to the time of detection is likely shorter than the time from any other QCD processes, such as hadronization and chiral symmetry breaking; therefore, it is apparently the most accurate one.

In the present calculations, full quantum statistics [13–17] and hadron resonances with masses up to 2.5 GeV [19] are taken into account. The strangeness degrees of freedom play an important role, especially at low μ_b or high $\sqrt{s_{NN}}$.

For the sake of completeness, we have also checked the same calculations but with the inclusion of a large number of possible missing states [57, 58]. We found that the thermodynamic quantities, especially the ones to which the present script is limited, show sensitivity to these missing states [59]. They are entering our calculations in the same manner as done for the PDG hadrons and resonances.

The missing states are resonances predicted theoretically but not yet confirmed experimentally. Their quantum numbers and physical characteristics are theoretically well known [60]. Basically, they are conjectured to greatly contribute to the fluctuations and the correlations, i.e., higher derivatives of the partition function, estimated in recent lattice QCD simulations [60]. These are the occasions where their contributions becomes unavoidable [57]. Another reason for adding the missing states is that they come up with additional degrees of freedom and considerable decay channels even to the hadrons and resonances which are subject of this present study.

For T_χ and μ_b, a comprehensive comparison between the thermal model calculations (curves) and the results deduced from the lattice QCD simulations (bands) [61, 62] and the Polyakov linear-sigma model (symbols with error bars) [63] is presented in Figure 2. Within their statistical and systematic certainties, there is an excellent agreement between the lattice QCD simulations (bands) [61, 62] and the Polyakov linear-sigma model (symbols) [63]. The reason why the lattice QCD simulations are limited to $\mu_q/T_\chi \leq 1$ is the so-called sign problem, and the difficulties which arise because of the importance of sampling becomes no longer possible. There are various attempts to anticipate this limitation: continuation from imaginary chemical potential, reweighting methods, applying complex Langevin dynamics, and Taylor expansions in the quark chemical potential μ_q [64].

We also find an excellent agreement between the thermal model calculations for the chemical freezeout parameters and the predictions deduced from the Polyakov linear-sigma model, especially at $\mu_b \gtrsim 300$MeV. At lower μ_b, the thermal model calculations seem to slightly overestimate T_χ.

This observed agreement would be taken as an evidence supporting the conclusion that the first-principle calculations likely result in the $T_\chi - \mu_b$ plane similar to that of the Polyakov linear-sigma model, especially at large μ_b, where the first-principle calculations are no longer applicable.

It is in order now to highlight a few details of the linear-sigma model, which is much simpler than QCD, but based on QCD symmetries as well [63, 65–70]. Originally, it

wasintended to describe the pion-nucleon interactions and the chiral degrees of freedom. A spinless scalar field σ_a and triplet pseudoscalar fields π_a are introduced in theory of quantized fields to the linear-sigma model, which is a low-energy effective model, in which the generators $T_a = \lambda_a/2$ with the Gell-Mann matrices λ_a and the real classical field forming an $\mathcal{O}(4)$ vector, $\vec{\Phi} = T_a(\vec{\sigma}_a, i\vec{\pi}_a)$, are included. The chiral symmetry is explicitly broken by a 3×3 matrix field $H = T_a h_a$, where h_a are the external fields. Accordingly, under $SU(2)_L \times SU(2)_R$ chiral transformation, such as $\Phi \longrightarrow L^{+}\Phi R$, the σ_a sigma fields acquire finite vacuum expectation values, which in turn break $SU(2)_L \times SU(2)_R$ down to $SU(2)_{L+R}$. These transformations produce a massive sigma particle and nearly massless Goldstone bosons, the pions. Therefore, the constituent quarks gain masses, as well, $m_q = gf_\pi$, where g is coupling and f_π is the pion decay constant. Also, the fermions can be introduced either as nucleons or as quarks. The σ fields under chiral transformations exhibit the same behaviour as that of the quark condensates; thus, σ can be taken as order parameters for the QCD chiral phase transition.

With the incorporation of the Polyakov-loop potential, the Lagrangian of the PLSM reads $\mathscr{L} = \mathscr{L}_{\bar{\psi}\psi} + \mathscr{L}_m - \mathscr{U}(\phi, \phi^0, T)$, where the first term stands for Lagrangian density of fermions with N_c color degrees-of-freedom, the second term gives the contributions of the mesonic fields, and finally the third term represents the Polyakov-loop potential incorporating the gluonic degrees-of-freedom and the dynamics of the quark-gluon interactions, i.e., deconfinement is also incorporated in this chiral model.

The questions which arise now are why PLSM reproduces well the nonperturbative lattice QCD simulations and why the PLSM agrees well with the thermal model calculations, especially for the freezeout boundary? The first question can be directly answered. PLSM incorporates both chiral and deconfinement QCD symmetries. On the other hand, it seems that both types of transitions are nearly coincident, especially at vanishing or small baryon chemical potentials. Within this region, both calculations are in excellent agreement with each other. At high temperatures, both chiral symmetry restoration and deconfinement transition produce almost free quarks and gluons, e.g., QGP. The reliability of the chiral effective model, PLSM, seems crucial, especially where lattice field theory is unavailable or the experimental results are not accessible yet.

The second question about the reasons why PLSM agrees well with the freezeout parameters deduced from the thermal model calculations can be answered as follows. First, at $\mu_b \gtrsim 300\text{MeV}$, where the lattice field theory likely suffers from the sign problem, it seems that both chiral and deconfinement boundaries become more and more distinguishable. It might be obvious that the critical temperature of the chiral phase transition would be smaller than that of the deconfinement transition, which in turn differs from the freezeout temperatures. Within these two limits, which should be subject to further studies, a temperature region is created, in which a phase of mixed hadron-QGP likely takes place. Last but not least, the $T_\chi - \mu_b$ plane of the Polyakov linear-sigma model [63] was determined under the condition of constant entropy density normalized to T^3 [21–23], i.e., likely manifesting the freezeout boundary. A future phenomenological study should be conducted in order to find out whether the condition of line-of-constant-physics gives results in agreement with the $T_\chi - \mu_b$ plane for deconfinement.

Now, it is in order to summarize some details about the two lattice QCD calculations (yellow and grey bands). [61, 62]. In Ref. [61], the crossover boundary separating the hadron gas from the quark gluon plasma phases at small baryon chemical potentials was calculated using a four times stout smeared staggered fermion action with dynamical up, down, strange, and charm quarks (2 + 1 + 1). This means that the two light quarks degenerate. The masses of light quarks and that of the strange quark mass are tuned such that the physical pion and Kaon mass over the pion decay constant are reproduced for every lattice spacing. For the gauge action, the tree-level Symanzik improvement was used. In order to overcome the sign problem, imaginary values of the chemical potential have been considered, which are then translated through analytic continuation to the real values of the baryon-chemical potentials. The continuum extrapolation is based on lattices with 10, 12, and 16 temporal dimensions. The curvature of $x = T_c(\mu_b)/T_c(\mu_b = 0)$ was estimated according to approaches $1 + ax$, $1 + ax + bx^2$, $(1 + ax)/(1 + bx))$, and $(1 + ax + bx)^{-1}$, where a and b are fit parameters. The corresponding critical temperature at $\mu_b = 0$ was estimated as 157 MeV, where vanishing strange density was assured.

In Ref. [62], the critical temperatures of chiral crossovers at vanishing and finite values of baryon (b), strangeness (s), electric charge (Q), and isospin (I) chemical potentials obtained in the continuum limit from lattice QCD calculations carried out for 2 + 1 highly improved staggered quarks (HISQ) and the tree-level improved Symanzik gauge action with two degenerate up and down dynamical quarks and a dynamical strange quark, with physical quark masses corresponding to physical pion and Kaon masses are presented. The temporal extents are varied from $N_\tau = 6$, 8, 12, and 16, going towards progressively finer lattice spacing. The critical temperatures have been parameterized as $T_c(\mu_x) = T_c(\mu_x = 0)[1 - \kappa_2^x(\mu_x/T_c(\mu_x))^2 - \kappa_4^x(\mu_x/T_c(\mu_x = 0))^4]$, where κ_2^x and κ_4^x are determined from Taylor expansions of chiral observables in μ_x. The corresponding critical temperature at $\mu_b = 0$ was estimated as 156.5 ± 1.5 MeV. At the chemical freeze-out of relativistic heavy-ion collisions and under thermal conditions, such as $\mu_s(T, \mu_b)$ and $\mu_Q(T, \mu_b)$ determined from strangeness neutrality and isospin imbalance, $\kappa_2^b = 0.012 \pm 0.004$ and $\kappa_4^b = 0.000 \pm 0.0004$.

4. Conclusions and Outlook

Among the various phases which take place in the strongly interacting matter under extreme conditions, we focused on the deconfinement and chemical freezeout boundaries. The authors compared results on T_χ and μ_b deduced from various heavy-ion experiments with recent lattice simulations, the effective QCD-like Polyakov linear-sigma model, and

the equilibrium thermal model. Along the entire freezeout boundary, we conclude that an excellent agreement between the thermal model calculations and the experiments is found. Also, the estimations deduced from the Polyakov linear-sigma model excellently agree with the thermal model calculations. It should be noted that at low baryon density or high energies, both deconfinement and chemical freezeout boundaries are likely coincident. Accordingly, we can also conclude that the lattice calculations for the deconfinement transition agree well with the Polyakov linear-sigma model, wherein both approaches to QCD symmetries are included. At a large baryon density or low energies, the two boundaries become distinguishable and probably form a phase in which hadrons and quark-gluon plasma likely coexist.

Based on the fact that the Polyakov linear-sigma model agrees well with the lattice QCD simulations, at least within the μ_b range of reliable simulations, a future phenomenological study should be conducted on the Polyakov linear-sigma model to find out whether the condition of line-of-constant-physics gives results in agreement with the $T_\chi - \mu_b$ plane for deconfinement. Furthermore, it intends to characterize the phase of mixed hadron-QGP and its possible predictions at the future facilities of FAIR and NICA as well as its astrophysical consequences.

Data Availability

The data used to support the findings of this study are included within the article and/or cited properly.

Conflicts of Interest

The authors declare that they have no conflicts of interest.

References

[1] T. Banks and A. Ukawa, "Deconfining and chiral phase transitions in quantum chromodynamics at finite temperature," *Nuclear Physics B*, vol. 225, p. 145, 1983.

[2] A. N. Tawfik, "Equilibrium statistical–thermal models in high-energy physics," *International Journal of Modern Physics A*, vol. 29, article 1430021, 2014.

[3] B. P. Abbot and LIGO Scientific Collaboration and Virgo Collaboration, "GW170817: observation of gravitational waves from a binary neutron star inspiral," *Physical Review Letters*, vol. 119, article 161101, 2017.

[4] D. D. Ivanenko and D. F. Kurdgelaidze, "Hypothesis concerning quark stars," *Astrophysics*, vol. 1, no. 4, pp. 251-252, 1965.

[5] M. Gyulassy and L. McLerran, "New forms of QCD matter discovered at RHIC," *Nuclear Physics A*, vol. 750, no. 1, pp. 30–63, 2005.

[6] W. Busza, K. Rajagopal, and W. van der Schee, "Heavy ion collisions: the big picture and the big questions," *Annual Review of Nuclear and Particle Science*, vol. 68, p. 339, 2018.

[7] C. Greiner, P. Koch-Steinheimer, F. M. Liu, I. A. Shovkovy, and H. Stoecker, "Chemical equilibration due to heavy Hagedorn states," *Journal of Physics G: Nuclear and Particle Physics*, vol. 31, no. 6, pp. S725–S732, 2005.

[8] B. Mueller and A. Schäefer, "Why does the thermal model for hadron production in heavy ion collisions work?," https://arxiv.org/abs/1712.03567.

[9] V. Vovchenko, M. I. Gorenstein, C. Greiner, and H. Stoecker, "Hagedorn bag-like model with a crossover transition meets lattice QCD," *Physical Review C*, vol. 99, no. 4, article 045204, 2019.

[10] L. D'Alessio, Y. Kafri, A. Polkovnikov, and M. Rigol, "From quantum chaos and eigenstate thermalization to statistical mechanics and thermodynamics," *Advances in Physics*, vol. 65, no. 3, pp. 239–362, 2016.

[11] G. Fast, R. Hagedorn, and L. W. Jones, "A statistical interpretation of large-angle elastic scattering," *Il Nuovo Cimento*, vol. 27, no. 4, pp. 856–859, 1963.

[12] G. Fast and R. Hagedorn, "Large-angle elastic scattering at high energies treated by a statistical model," *Il Nuovo Cimento*, vol. 27, no. 1, pp. 208–217, 1963.

[13] F. Karsch, K. Redlich, and A. Tawfik, "Hadron resonance mass spectrum and lattice QCD thermodynamics," *The European Physical Journal C*, vol. 29, p. 549, 2003.

[14] F. Karsch, K. Redlich, and A. Tawfik, "Thermodynamics at non-zero baryon number density: a comparison of lattice and hadron resonance gas model calculations," *Physics Letters B*, vol. 571, no. 1-2, pp. 67–74, 2003.

[15] K. Redlich, F. Karsch, and A. Tawfik, "Heavy-ion collisions and lattice QCD at finite baryon density," *Journal of Physics G: Nuclear and Particle Physics*, vol. 30, no. 8, pp. S1271–S1274, 2004.

[16] A. Tawfik, "QCD phase diagram: A comparison of lattice and hadron resonance gas model calculations," *Physics Review D*, vol. 71, no. 5, article 054502, 2005.

[17] A. Tawfik and D. Toublan, "Quark-antiquark condensates in the hadronic phase," *Physics Letters B*, vol. 623, no. 1-2, pp. 48–54, 2005.

[18] M. Tanabashi, K. Hagiwara, K. Hikasa et al., "Review of Particle Physics," *Physics Review D*, vol. 98, no. 3, article 030001, 2018.

[19] J. Beringer and Particle Data Group, *Physics Review D*, vol. 86, article 010001, 2012.

[20] A. N. Tawfik and E. Abbas, "Thermal description of particle production in Au-Au collisions at RHIC energies (STAR)," *Physics of Particles and Nuclei Letters*, vol. 12, no. 4, pp. 521–531, 2015.

[21] A. Tawfik, M. Y. El-Bakry, D. M. Habashy, M. T. Mohamed, and E. Abbas, "Possible interrelations among chemical freeze-out conditions," *International Journal of Modern Physics E*, vol. 25, no. 3, article 1650018, 2016.

[22] A. Tawfik, "A universal description for the freezeout parameters in heavy-ion collisions," *Nuclear Physics A*, vol. 764, pp. 387–392, 2006.

[23] A. Tawfik, "Condition driving chemical freeze-out," *Europhysics Letters*, vol. 75, no. 3, pp. 420–426, 2006.

[24] A. Tawfik, "Chemical freeze-out and higher order multiplicity moments," *Nuclear Physics A*, vol. 922, pp. 225–236, 2014.

[25] A. Tawfik, "Modified Newton's Law of gravitation due to minimal length in quantum gravity," *Advances in High Energy Physics*, vol. 2013, Article ID 574871, 7 pages, 2013.

[26] A. Tawfik, "Constant-trace anomaly as a universal condition for the chemical freeze-out," *Physics Review C*, vol. 88, no. 3, article 035203, 2013.

[27] A. N. Tawfik, H. Yassin, and E. R. A. Elyazeed, "Chemical freeze-out in Hawking-Unruh radiation and quark-hadron transition," *Physics Review D*, vol. 92, no. 8, article 085002, 2015.

[28] A. Tawfik, "Influence of strange quarks on the QCD phase diagram and chemical freeze-out," *Journal of Physics G: Nuclear and Particle Physics*, vol. 31, no. 6, pp. S1105–S1110, 2005.

[29] G. Agakishiev, A. Balanda, D. Belver et al., "Dielectron production in Ar + KCl collisions at 1.76AGeV," *Physical Review C*, vol. 84, no. 1, article 014902, 2011.

[30] V. V. Begun, V. Vovchenko, and M. I. Gorenstein, "Updates to the p+p and A+A chemical freeze-out lines from the new experimental data," *Journal of Physics Conference Series*, vol. 779, article 012080, 2017.

[31] M. Lorenz, "Reviewing hadron production at SIS energies featuring the new HADES Au+Au data," *Nuclear Physics A*, vol. 931, pp. 785–789, 2014.

[32] N. Abgrall, A. Aduszkiewicz, Y. Ali et al., "Measurement of negatively charged pion spectra in inelastic p+p interactions at p_{lab} = 20, 31, 40, 80 and 158 GeV/c," *The European Physical Journal C*, vol. C74, article 2794, 2014.

[33] G. Agakishiev, O. Arnold, D. Belver et al., "Associate K^0 production in p+p collisions at 3.5 GeV: The role of $\Delta(1232)^{++}$," *Physics Review C*, vol. 90, article 015202, 2014.

[34] G. Agakishiev, O. Arnold, D. Belver et al., "$K^*(892)^+$ production in proton-proton collisions at E_{beam} = 3.5 GeV," *Physics Review C*, vol. 92, article 024903, 2015.

[35] T. Anticic, B. Baatar, D. Barna et al., "System-size dependence of Λ and Ξ production in nucleus-nucleus collisions at 40A and 158A GeV measured at the CERN Super Proton Synchrotron," *Physics Review C*, vol. 80, article 034906, 2009.

[36] T. Anticic, B. Baatar, D. Barna et al., "Energy dependence of transverse momentum fluctuations in Pb+Pb collisions at the CERN Super Proton Synchrotron (SPS) at 20A to 158A GeV," *Physical Review C*, vol. 79, article 044904, 2009.

[37] V. Vovchenko, M. Gorenstein, L. Satarov, and H. Stöcker, *Chemical Freeze-out Conditions in Hadron Resonance Gas, in New Horizons in Fundamental Physics*, Springer, 2017.

[38] C. Alt, T. Anticic, B. Baatar et al., "Ω^- and $\bar{\Omega}^+$ Production in Central Pb+Pb collisions at 40 and 158A GeV," *Physical Review Letters*, vol. 94, article 192301, 2005.

[39] I. Kraus and the NA49 Collaboration, "System size dependence of strange particle yields and spectra at $\sqrt{s_{\mathrm{NN}}} = 17.3$ GeV," *Journal of Physics G: Nuclear and Particle Physics*, vol. 31, no. 4, pp. S147–S154, 2005.

[40] M. Floris, "Hadron yields and the phase diagram of strongly interacting matter," *Nuclear Physics A*, vol. 931, pp. 103–112, 2014.

[41] A. Andronic, P. Braun-Munzinger, K. Redlich, and J. Stachel, "Decoding the phase structure of QCD via particle production at high energy," *Nature*, vol. 561, no. 7723, pp. 321–330, 2018.

[42] B. Abelev, J. Adam, D. Adamová et al., "K^0_S and Λ Production in Pb-Pb Collisions at $\sqrt{s_{\mathrm{NN}}}$ = 2.76 TeV," *Physical Review Letters*, vol. 111, no. 22, article 222301, 2013.

[43] D. Alexandre and ALICE Collaboration, "Multi-strange baryon production in pp, p–Pb and Pb–Pb collisions measured with ALICE at the LHC," *Nuclear Physics A*, vol. 931, pp. 1093–1097, 2014.

[44] ALICE Collaboration, "$K^*(892)^0$ and $\phi(1020)$ production in Pb-Pb collisions at $\sqrt{s_{\mathrm{NN}}}$ = 2.76 TeV," *Physical Review C*, vol. 91, no. 2, article 024609, 2015.

[45] ALICE Collaboration, "${}^3_\Lambda\mathrm{H}$ and ${}^3_\Lambda\bar{\mathrm{H}}$ production in Pb-Pb collisions at $\sqrt{s_{\mathrm{NN}}}$ = 2.76 TeV," https://arxiv.org/abs/1506.08453.

[46] ALICE Collaboration, "Production of ^{4}He and ${}^4\overline{\mathrm{He}}$ in Pb-Pb collisions at $\sqrt{s_{\mathrm{NN}}}$ = 2.76 TeV at the LHC," https://arxiv.org/abs/1710.07531.

[47] B. Abelev, J. Adam, D. Adamová et al., "Pion, Kaon, and Proton production in central Pb-Pb collisions at $\sqrt{s_{\mathrm{NN}}}$ = 2.76 TeV," *Physical Review Letters*, vol. 109, no. 25, article 252301, 2012.

[48] J. Cleymans, H. Oeschler, K. Redlich, and S. Wheaton, "Comparison of chemical freeze-out criteria in heavy-ion collisions," *Physical Review C*, vol. 73, no. 3, article 034905, 2006.

[49] C. Adler, Z. Ahammed, C. Allgower et al., "Centrality Dependence of High-ρT Hadron Suppression in Au+Au Collisions at $\sqrt{s_{\mathrm{NN}}}$ = 130 GeV," *Physical Review Letters*, vol. 89, no. 20, article 202301, 2002.

[50] C. Adler, Z. Ahammed, C. Allgower et al., "Multiplicity distribution and spectra of negatively charged hadrons in Au+Au Collisions at $\sqrt{s_{\mathrm{NN}}}$ = 130 GeV," *Physical Review Letters*, vol. 87, no. 11, p. 112303, 2001.

[51] J. Adams, M. M. Aggarwal, Z. Ahammed et al., "Identified hadron spectra at large transverse momentum in $p + p$ and $d + $ Au collisions at $\sqrt{s_{\mathrm{NN}}}$ = 200 GeV," *Physics Letters B*, vol. 637, no. 3, pp. 161–169, 2006.

[52] J. Velkovska, "P_t distributions of identified charged hadrons measured with the PHENIX experiment at RHIC," *Nuclear Physics A*, vol. 698, no. 1-4, pp. 507–510, 2002.

[53] J. Adams, M. M. Aggarwal, Z. Ahammed et al., "Experimental and theoretical challenges in the search for the quark–gluon plasma: The STAR Collaboration's critical assessment of the evidence from RHIC collisions," *Nuclear Physics A*, vol. 757, no. 1-2, pp. 102–183, 2005.

[54] H. Oeschler, "Pion and kaon production as a probe for hot and dense nuclear matter," in *Hadrons in Dense Matter and Hadrosynthesis*, J. Cleymans, H. B. Geyer, and F. G. Scholtz, Eds., vol. 516 of Lecture Notes in Physics, p. 1, Springer, Berlin, Heidelberg, 1999.

[55] V. I. Yukalova and E. P. Yukalov, "Critical temperature in weakly interacting multicomponent field theory," *EPJ Web of Conferences*, vol. 138, article 03011, 2017.

[56] K. A. Bugaev, V. V. Sagun, A. I. Ivanytskyi et al., "New signals of quark-gluon-hadron mixed phase formation," *The European Physical Journal A*, vol. 52, p. 227, 2016.

[57] P. Man Lo, M. Marczenko, K. Redlich, and C. Sasaki, "Missing baryonic resonances in the Hagedorn spectrum," *The European Physical Journal A*, vol. 52, p. 235, 2016.

[58] J. Noronha-Hostler, "Implications of missing resonances in heavy ions collisions," in *Workshop on Excited Hyperons in QCD Thermodynamics at Freeze-Out (YSTAR2016) Mini-Proceedings*, pp. 118–127, Newport News, VA,USA, November 2016.

[59] S. Capstick and N. Isgur, "Baryons in a relativized quark model with chromodynamics," *Physics Review*, vol. 34, pp. 2809–2835, 1986.

[60] A. Bazavov, H. T. Ding, P. Hegde et al., "Additional Strange Hadrons from QCD Thermodynamics and Strangeness Freezeout in Heavy Ion Collisions," *Physical Review Letters*, vol. 113, no. 7, article 072001, 2014.

[61] R. Bellwied, S. Borsanyi, Z. Fodor et al., "The QCD phase diagram from analytic continuation," *Physics Letters B*, vol. 751, pp. 559–564, 2015.

[62] A. Bazavov, H.-T. Ding, P. Hegde et al., "Chiral crossover in QCD at zero and non-zero chemical potentials," *Physics Letters B*, vol. 795, pp. 15–21, 2019.

[63] A. Tawfik, N. Magdy, and A. Diab, "Polyakov linear SU(3) σ model: Features of higher-order moments in a dense and thermal hadronic medium," *Physics Review C*, vol. 89, article 055210, 2014.

[64] O. Philipsen, "Lattice QCD at non-zero temperature and baryon density," in *Modern Perspectives in Lattice QCD: Quantum Field Theory and High Performance Computing Lecture Notes of the Les Houches Summer School: Volume 93, August 2009*, pp. 273–330, Oxford University Press, 2011.

[65] A. N. Tawfik and A. M. Diab, "Polyakov SU(3) extended linear-σ model: Sixteen mesonic states in chiral phase structure," *Physics Review C*, vol. 91, no. 1, article 015204, 2015.

[66] A. M. A. A. Diab and A. N. Tawfik, "Quark-hadron phase structure of QCD matter from SU(4) Polyakov linear sigma model," *EPJ Web of Conferences*, vol. 177, article 09005, 2018.

[67] A. Nasser Tawfik and A. Magied Diab, "Black hole corrections due to minimal length and modified dispersion relation," *International Journal of Modern Physics A*, vol. 30, article 1550059, 2015.

[68] A. N. Tawfik, A. M. Diab, and M. T. Hussein, "Quark–hadron phase structure, thermodynamics, and magnetization of QCD matter," *Journal of Physics G: Nuclear and Particle Physics*, vol. 45, no. 5, article 055008, 2018.

[69] A. N. Tawfik, A. M. Diab, and M. T. Hussein, "SU(3) Polyakov linear-sigma model: Conductivity and viscous properties of QCD matter in thermal medium," *International Journal of Modern Physics A*, vol. 31, no. 34, article 1650175, 2016.

[70] A. N. Tawfik, A. M. Diab, and M. T. Hussein, "Chiral phase structure of the sixteen meson states in the *SU*(3) Polyakov linear-sigma model for finite temperature and chemical potential in a strong magnetic field," *Chinese Physics C*, vol. 43, article 034103, no. 3, 2019.